Organic & Biomolecular Chemistry

QM/MM Modeling of Class A β-Lactamases Reveals Distinct Acylation Pathways for Ampicillin and Cefalexin

Journal:	*Organic & Biomolecular Chemistry*
Manuscript ID	OB-COM-08-2021-001593.R1
Article Type:	Communication
Date Submitted by the Author:	22-Sep-2021
Complete List of Authors:	Song, Zilin; Southern Methodist University, Department of Chemistry Trozzi, Francesco; Southern Methodist University, Department of Chemistry Palzkill, Timothy; Baylor College of Medicine, Pharmacology Tao, Peng; Southern Methodist University, Department of Chemistry

SCHOLARONE™
Manuscripts

QM/MM Modeling of Class A β-Lactamases Reveals Distinct Acylation Pathways for Ampicillin and Cefalexin

Zilin Song,[a] Francesco Trozzi,[a] Timothy Palzkill,[b] Peng Tao[a,c,*]

[a] Department of Chemistry, Center for Research Computing, Center for Drug Discovery, Design, and Delivery (CD4), Southern Methodist University, Dallas, Texas 75205, United States;

[c] orcid.org/0000-0002-2488-0239

[b] From the Verna and Marrs McLean Department of Biochemistry and Molecular Biology and Department of Pharmacology and Chemical Biology, Baylor College of Medicine, Houston, Texas 77030, United States; orcid.org/0000-0002-5267-0001;

*Correspondence: ptao@smu.edu

Abstract

Efficient mechanism-based design of antibiotics that are not susceptible to β-lactamases is hindered by the lack of comprehensive knowledge on the energetic landscapes for the hydrolysis of various β-lactams. Herein, we adopted efficient quantum mechanics/molecular mechanics simulations to explore the acylation reaction catalyzed by CTX-M-44 (Toho-1) β-lactamase. We show that the catalytic pathways for β-lactam hydrolysis are correlated to substrate scaffolds: using Glu166 as the only general base for acylation is viable for ampicillin but prohibitive for cefalexin. The present computational workflow provides quantitative insights to facilitate the optimization of future β-lactam antibiotics.

Antibiotic resistance undermines the effective treatment of bacterial infections. The application of β-lactam drugs has elevated many bacterial strains to inactivate common β-lactam based antibiotics families. One major source of β-lactam resistance stems from β-lactamases, bacterially-produced enzymes that effectively hydrolyze β-lactam drugs.[1–3] β-lactamases are generally classified into four groups: classes A, C, D are serine-based, and class B are zinc-based. Class A serine β-lactamases (ASβLs) represent a severe threat due to their prevalence in infectious strains and affinity to a wide range of β-lactams.[4,5] The inactivation of β-lactams by ASβLs has been extensively explored by pioneering computational and experimental studies. Conserved in most ASβLs, a widely-accepted catalytic mechanism has been proposed that β-lactamase-promoted hydrolysis is a serine-mediated acylation-deacylation process.[6–19] The acylation pathways have shown flexibility as this process could be mediated by either Lys73 or Glu166 acting as the general base (Fig 1a).[6–8] While the acylation process is believed to be conserved in all ASβLs, their catalytic efficiency (k_{cat}/K_M) against different β-lactam substrates has been shown to be diverse.[2,3,9] Among hundreds of β-lactam-based antibiotics being developed, the most successful efforts involve engineering the β-lactam cyclic scaffold.[20] In this regard, understanding the underlying interaction landscapes resulting from modifications on substrate structures can be informative for future optimization and design of novel antibiotic series.

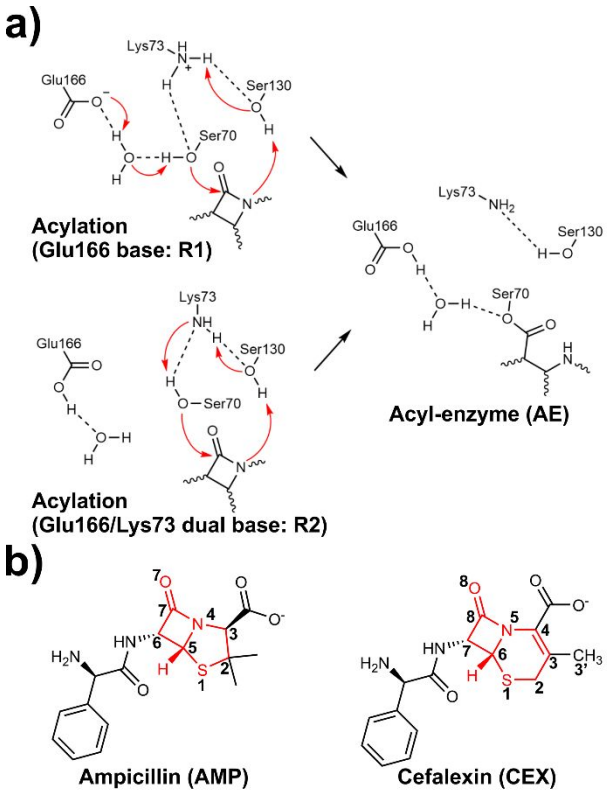

Figure 1. Mechanisms of acylation in ASβLs and structures of the model substrates. (a) The general mechanism of β-lactam acylation mediated by ASβL; (b) Structures of ampicillin (AMP) and cefalexin (CEX).

CTX-M is a representative ASβL group and has been identified as an immediate menace to commonly prescribed β-lactam antibiotics.[4] The CTX-M enzyme class is characterized by its enhanced catalytic efficiency (k_{cat}/K_M) against cephalosporin antibiotic families.[5] The hydrolysis of most cephalosporins deviates from that of other β-lactams by bearing a leaving group at its C3' position. Expelling the C3' leaving group would trigger a series of rearrangements, allowing its dihydrothiazine nitrogen to stay as an unprotonated imine after the acylation. However, an exception is cefalexin (CEX) which adopts a C3' methyl as a poor leaving group (Fig. 1b); The protonation of the CEX cephem amine is thus inevitable. CEX also poses enhanced resistance against CTX-M hydrolysis compared to other

early generations of penicillin or cephalosporins. In particular, Nitanai *et al.*[9] showed that the catalytic efficiency (k_{cat}/K_M) of CEX hydrolysis mediated by Toho-1 (also known as CTX-M-44) is 0.119 μM^{-1} s^{-1}, which is 17-fold lower than that of ampicillin (AMP, 2.11 μM^{-1} s^{-1}). Whereas AMP and CEX structurally differ only in their signature penam/cephem bicyclic rings (Fig. 1b), the cephem scaffold of CEX evidently showed higher hydrolysis resistance even to the CTX-M enzyme class.

Pioneering computational efforts applying hybrid Quantum Mechanical/Molecular Mechanical (QM/MM) techniques have provided fruitful insights into antibiotic resistance driven by ASβLs.[6–8] Compared to other methods, the QM/MM Chain-of-States (CoS) approaches[21–24] are inherently advantageous for computational efficiency and accuracy. As the CoS methods optimize the transition path in the original conformational space, exhaustive exploration in the reaction-coordinates or collective-variables reduced space can be avoided. Moreover, we demonstrated in a recent study[11] that the constraint-based Replica Path Method[21,22] optimized minimum energy pathways (MEPs) could provide barrier heights that are compatible to experimentally determined k_{cat} for ASβL-catalyzed hydrolysis. In this study, the acylation pathways of AMP and CEX hydrolysis in Toho-1 was investigated using QM/MM CoS calculations.

The high-resolution crystal structures of Toho-1/benzylpenicillin (PDB entry: 5KMW, 1.10 Å)[10] and Toho-1/cephalothin (PDB entry: 2ZQ9, 1.07 Å)[9] acyl-enzyme complexes were used as template systems to create structures for Toho-1/AMP and Toho-1/CEX complexes. The topology files of AMP and CEX were derived from CHARMM General Force Field (CGenFF)[25–27]. The ligand topologies in the template systems were then substituted to create initial structures for Toho-1/AMP and Toho-1/CEX complexes. As Lys73 and Glu166 are both potential general bases during the acylation step, systems with alternative protonation states on Lys73 and Glu166 were prepared to account for acylation pathways via different general base residues: first with protonated Lys73 and deprotonated Glu166 (noted as R1), and the other

with deprotonated Lys73 and protonated Glu166 (noted as R2). The protonation states of other titratable residues are assigned referring to additional pKa calculations (Table S1) and neutron diffraction data of the *apo*-state Toho-1[12]. A total of 4 enzyme-ligand models were created, protonated, optimized, and equilibrated using a semi-empirical QM/MM scheme with the third-order Density Functional Tight Binding theory with the 3OB parameter set (DFTB3/3OB)[28,29] as the QM potential and CHARMM36 force field (C36)[30] as the MM counterpart (see Supporting Information, SI, Fig. S1, Fig. S2 for details). The interatomic distances between the key reacting heavy atoms during a 100 ps molecular dynamic simulation using the DFTB3/3OB/C36 potential are shown in Table 1; it is noted that the distribution of key reacting distances does not significantly differ between the 2 systems. The initial structures of the pathway calculations were selected as the snapshots that have the minimal inter-heavy-atom distances between the reacting functional groups of the four residues (Ser70, Lys73, Ser130, and Glu166), the catalytic water and the β-lactam.

Table 1. The mean interatomic distances between key reacting heavy atoms in the DFTB3/3OB/C36 dynamics. Parenthesis denote the standard deviation (unit: Å).

Atom pairs	Toho/AMP:R1	Toho/CEX:R1	Toho/AMP:R2	Toho/CEX:R2
Ser70 Oγ – AMP C7 or CEX C8	2.43 (0.17)	2.58 (0.18)	2.44 (0.17)	2.57 (0.18)
Lys73 Nζ – Ser130 Oγ	2.85 (0.15)	2.95 (0.32)	3.07 (0.25)	3.15 (0.32)
Ser130 Oγ – AMP N4 or CEX N5	3.60 (0.23)	3.86 (0.26)	3.67 (0.31)	3.63 (0.31)
Ser70 Oγ – $Water_{cat}$ O	2.65 (0.10)	2.65 (0.09)	–	–
Glu166 Oε2 – Watercat O	3.06 (0.23)	2.77 (0.17)	–	–
Ser70 Oγ – Lys73 Nζ	–	–	2.88 (0.13)	2.93 (0.17)

A total of 5 structures (noted as Toho/AMP: R1, R2, and Toho/CEX: R1, R1a, R2) were chosen from the production trajectories. These 5 frames were then subjected to calculations at Density Functional Theory (DFT) level. The DFT QM region covers important active site fragments: β-lactams, the catalytic water, the surrounding residues (Ser70, Lys73, Ser130, Glu166, Asn170, Lys234, Thr235, Ser237), together with a surrounding solvent molecule for the reaction pathway calculations. The hybrid density functional B3LYP[31] was used in conjunction with Pople's 6-31G double ζ basis set[32] for the QM atoms (B3LYP/6-31G/C36). The experimentally known stable states (reactant and acyl-enzyme) were first subjected to geometry optimizations at the DFT/MM level. The optimized states were then connected by a series of replicated conformations (replicas) that linearly intercepted the Cartesian space. The Replica Path Method with holonomic constraints[21] implemented in CHARMM[33] was applied for all pathway optimizations through its interface[34] to Q-Chem[35]. In order to comprehensively explore the stable intermediates along the reaction, the replicas on the initial MEPs were independently minimized to the nearest local minimum states. The final MEPs were then obtained by re-optimizing the chain-of-replicas that connects the local minimums identified from the initial pathways. The energetic profiles on the B3LYP/6-31G/C36 optimized MEPs were further refined with the augmented 6-31++G** basis set[36]. Lonsdale *et al*.[37,38] proposed that the contribution from the dispersion effect is critical to accurately account for enzymatic reaction profiles, therefore the D3 dispersion correction of Grimme[39] was also applied in the single point energy calculations (B3LYP-D3/6-31++G**/C36). The locations of the transition states are approximated by the replica with the highest energy on the optimized minimal energy path. This dual-level DFT/MM workflow has been previously validated for closely resembling the catalytic barriers in similar ASβL systems.[11] The ChElPG scheme[40] was employed for the charge population analysis along the chain-of-states.

Pioneering theoretical studies proposed that the acylation of β-lactams could be mediated by either Glu166 along or concertedly with Lys73. Hermann *et al*.[6] first reported that the acylation reaction could be mediated using Glu166 as the basic proton host in ASβL hydrolysis. In a similar ASβL/penam system, Meroueh *et al*.[8] further proposed that Lys73 is a viable alternative for the general base that accepts the Ser70 hydroxyl proton. Augmented by extensive Machine-Learning regression analysis, our previous work[11] on TEM-1 acylation pathways bridged the discrepancies between the energetics reported from the above pioneer studies. In the present study, both pathways for acylation were investigated for AMP and CEX.

The optimized reactant structures of Toho/AMP differ from Toho/CEX by the hydrogen bonding networks between the penam/cephem carboxylate and the residues Thr235, Ser237 (Fig 2, Fig. S3). Practically, the Ser237 hydroxyl is generally outside of the H-bonding region of the AMP carboxylic group. The reactant configuration is therefore stabilized by a water molecule serving as the H-bond bridge between the Ser237 hydroxyl and the AMP carboxylate (Toho/AMP:R1, Fig. 2a). Meanwhile, the CEX adopts a more flexible binding pattern: the hydroxyl group from Ser237 could either form direct hydrogen interacting to the substrate carboxyl group (Toho/CEX:R1, Fig. 2b) or to a solvent water molecule (Toho/CEX:R1a, Fig. 2c). The superimposed conformations of the reactant states show that the QM residues, the substrates and the catalytic water share a similar orientation (Fig. S4), indicating that the optimized reactant structures are in the equivalent stationary potential energy state. As for the product acyl-enzyme states, Vandavasi *et al.*[12] observed two Lys73 conformers in the perdeuterated acyl-enzyme complex of Toho(Glu166Ala)/cefotaxime (PDB entry: 5A93, 2.20 Å). In our study, the conformations of all AE1 states agree with the B conformer that carries a deprotonated Lys73 amine with its sidechain resting in an extended configuration (Fig. S5). Notably, we observed an alternative Lys73 deprotonated acyl-enzyme local minimum state (AE2) on all acylation pathways. The AE2 states

slightly differ from the AE1 states by the configuration of the deprotonated Lys73 amino (Fig. S6): the AE2 Lys73 Nζ adopts an extra hydrogen interaction to Ser70 Oγ, while the AE1 Lys73 does not form the H-bonds to the acyl-serine complex. While the conversion between AE1 and AE2 are found to be barrier-less on all acylation pathways, we note that the AE1 states are shown to be slightly more energetically favorable as their energies are generally 2-4 kcal mol^{-1} lower than the AE2 states (Table S2).

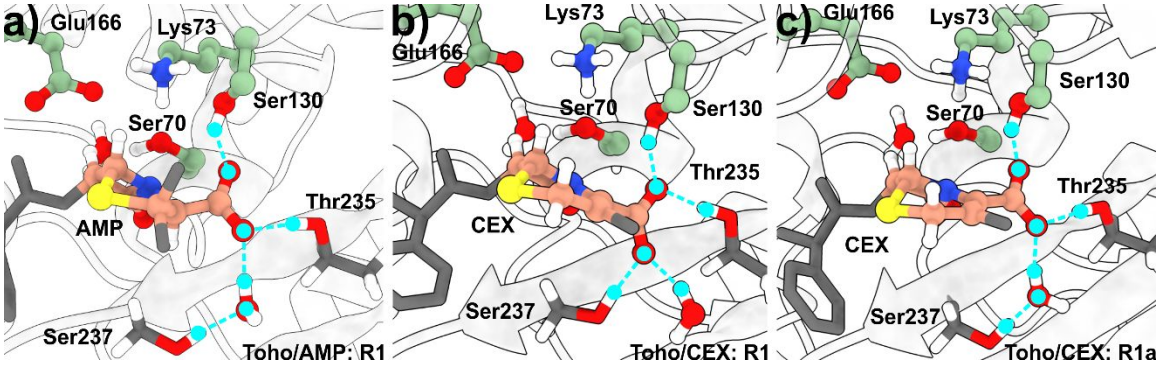

Figure 2. Conformations of R1 reactant states. The conformations of (a) Toho/AMP:R1; (b) Toho/CEX:R1; (c) Toho/CEX:R1a. The hydrogen bonding interactions are noted as blue dashed lines.

Our calculated Toho/AMP acylation pathways (Fig. 3a) closely resemble the potential energy landscapes reported by Meroueh *et al.*[8]: the energy barrier for the acylation using Glu166 as general base (14.0 kcal mol^{-1}) is moderately higher than that of Lys73/Glu166 concerted base (8.7 kcal mol^{-1}). The Toho/AMP acylation pathways agree with both acylation mechanisms, indicating that either Lys73 or Glu166 could mediate the acylation process in Toho/AMP hydrolysis. The ChElPG charge profiles of the Toho/AMP pathways align with the intuitive understanding of the reaction mechanism. As shown in Fig. 3b and 3c, the decreasing charge population on AMP O7 between replica 20 to 27 is synergetic to the increasing charge on Ser70 Oγ, suggesting the formation of tetrahedral intermediate (with a formal

158 charge of -1 on AMP O7) during the serine addition. Furthermore, the locations of maximal charge
159 profiles on AMP N4 are also correlated with the replica with the highest energy along the reaction
160 progress, showing that the protonation of AMP N4 is strongly correlated with the rate of acylation,
161 agreeing with previous observations[11].
162

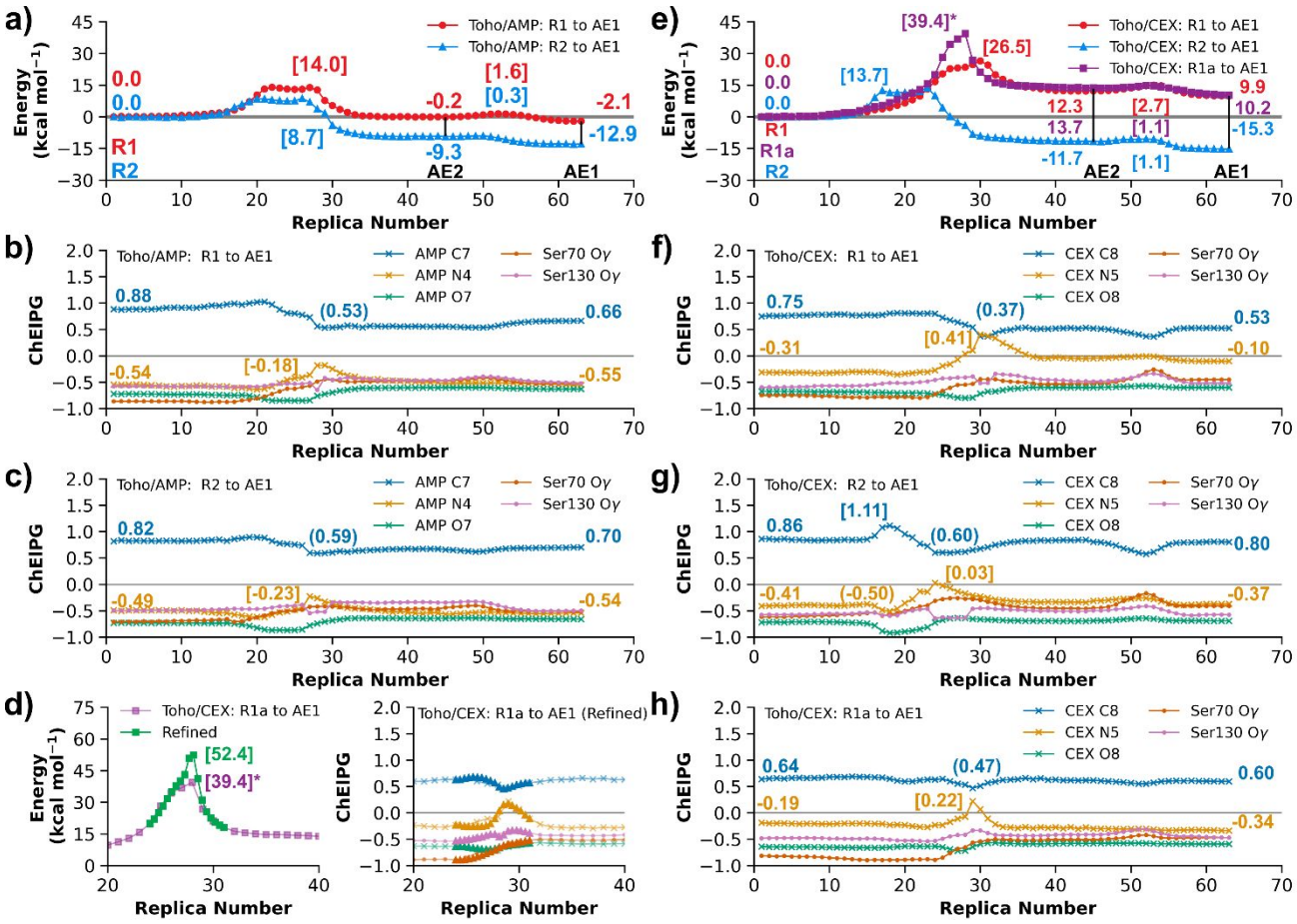

163

164 **Figure 3. Energy profiles and the ChElPG charges of key atoms along the acylation pathways in**
165 **Toho-1 hydrolysis.** (a) The acylation profiles of Toho/AMP; The ChElPG charges along (b) the
166 Toho/AMP: R1 to AE1 pathway, and (c) the Toho/AMP: R2 to AE1 pathway; (d) The energy profile
167 and the ChElPG charge profiles of the refined Toho/CEX: R1a to AE1 pathways, which is calculated
168 from inserting 18 replicas between replica 24 and 31 (see SI); (e) The acylation profiles of Toho/CEX;
169 The ChElPG charges along (f) the Toho/CEX: R1 to AE1 pathway, (g) the Toho/CEX: R2 to AE1

pathway, and (h) the Toho/CEX: R1a to AE1 pathway. The vertical black solid lines in (a) and (d) indicate the location of AE1 and AE2. Numbers in parentheses and brackets denote the local minimum and maximum values of important states along the reaction path. Note that only ChElPG charge values of β-lactam carbonyl carbon (blue) and nitrogen (orange) are shown in (b), (c), (f), (g), (h). See also Table S3-S7 for detailed replica-wise energy components and ChElPG charges on key atoms.

However, Toho/CEX acylation demonstrates a different catalytic mechanism, as shown in Fig. 3e. The acylation barrier using Glu166 as the general base is prohibitively high (26.5 kcal mol^{-1}). In particular, the corresponding barrier further increases to 52.4 kcal mol^{-1} when cefalexin substrate adopts a similar binding pattern as ampicillin (Toho/CEX:R1a to AE1, Fig. 3d). These leave Lys73 as the inevitable candidate to mediate deprotonation of the Ser70 hydroxyl during CEX acylation, which confers an energetic barrier of 13.7 kcal mol^{-1} (Toho/CEX:R2 to AE1). Further mechanistic insights can be derived from the ChElPG charge profiles. On the Glu166-mediated Toho/CEX acylation pathways (Fig. 3e, 3g, 3h), a stable tetrahedral intermediate indicated by the temporarily decreased charge on β-lactam carbonyl oxygen (as in the corresponding Toho/AMP pathways) is less synergetic to the formation of the tetrahedral intermediate. Moreover, the charge on the cephem nitrogen is largely increased to 0.41 (Fig. 3e) and 0.22 (Fig. 3g) upon the barrier replica, which evidently suggests its poor proton affinity to accept the proton transfer from Ser130. Alternatively, the dual-base mediated Toho/CEX: R2 to AE1 pathways (Fig. 3f) demonstrates a similar charge profile to the corresponding AMP acylation pathway. Interestingly, an increase of ChElPG charge on CEX C8 is seen uniquely upon the formation of tetrahedral intermediate on this pathway (Fig. 3f, replica 18). Intuitively, the lone pair on Ser70 Oγ in the R2 configurations are oriented towards the ligand carbonyl carbon, potentially activating the conjugated π orbital on the β-lactam bicyclic. While the π-conjugation in AMP (N4-

C7=O8) is localized to the β-lactam scissile C-N bond, it is extended along the cephem bicyclic (C3=C4-N5-C8=O8) in CEX. The temporary charge increment on CEX C8 can therefore be interpreted as the consequence of breaking the more delocalized π-conjugation on the cephem scissile bond during the nucleophilic attack of Ser70 Oγ. Accordingly, this explanation is also supported by the observation that the tetrahedral intermediates on Toho/AMP and Toho/CEX pathways do not significantly differ from each other in terms of heavy atom conformations (Fig. S7).

The computational barriers are further correlated with experimental kinetic studies (Table 2). Nitanai *et al.*[9] reported that the catalytic barrier (calculated from k_{cat}) of Toho/AMP hydrolysis is ~14.9 kcal mol^{-1}, slightly lower by ~1.7 kcal mol^{-1} than that of CEX (~16.6 kcal mol^{-1}). In our calculations, both acylation barriers for Toho/AMP are sufficiently lower than the experimentally determined catalytic barrier, suggesting that the acylation mechanism previously developed for ASβLs are applicable to Toho-1/AMP as well. In contrast, the only viable reaction pathway for CEX is the Lys73/Glu166 dual base mechanism. The pathway that uses Glu166 as the only general base greatly exceeded the experimental barrier (16.6 kcal mol^{-1}) by 9.9 kcal mol^{-1}.

Table 2. The catalytic barriers of ampicillin and cefalexin hydrolysis in Toho-1.

Source [a]	Systems	Energy barriers (kcal mol^{-1})	Method [b]
Shimizu-Ibuka *et al.*[13, c]	Toho-1/AMP	15.5	303.15K, Exp
Nitanai *et al.*[9]	Toho-1/AMP	14.9	303.15K, Exp
This study.	**Toho-1/AMP**	**8.7 / 14.0** [d]	**B3LYP-D3, CoS**
Nitanai *et al.* [9]	Toho-1/CEX	16.6	303.15K, Exp
This study.	**Toho-1/CEX**	**13.7 / 26.5** [d]	**B3LYP-D3, CoS**

[a] Bold entries are computational results from this study;

[b] The experimental (Exp) catalytic barrier of Toho/AMP were derived from k_{cat} via the Eyring equations, the acylation barrier of Toho/CEX were derived from the ratio of k_{cat}/K_M to Toho/AMP;
[c] This study used the wild-type Toho-1 as the enzyme host while others used the Arg274Asn/Arg276Asn Toho-1 mutant as the enzyme host;
[d] Values before "/" report the barrier of the Lys73/Glu166 concerted base acylation pathway. Values after "/" report the Glu166 sole base acylation pathway.

In this study, we demonstrate that the AMP and CEX acylation energy landscapes differ from each other during Toho-1 hydrolysis. Pioneering computational mechanistic studies[6,8] suggested that acylation could be mediated by either Glu166 solely or concertedly with Lys73 as the general proton acceptor(s). In our calculations of both systems, the R1 pathway, which is mediated solely by Glu166 as the base, confers a higher (potential) energy barrier than the R2 pathways. Using a cefotaxime bound Toho-1 system, Langan *et al.*[14] showed that the transition from R1 to R2 confers a free energy barrier of ~5 kcal mol^{-1}, suggesting fast transitions between R1 and R2. This observation leads to the question of whether the R1 acylation pathway is mechanistically important in Toho-1 (or other ASβLs) catalysis. Herein, the R1 acylation pathway is shown to be energetically prohibitive for CEX (Fig. 3e, Table 2), leaving the Lys73/Glu166 dual base mechanism as the main viable pathway for its acylation. In the case of AMP, whereas the investigated acylation barrier via the Glu166 sole base mechanism is sufficiently lower than the experimentally determined kinetics (Table 2), the viability of the R1 pathway is not evidently clear from the potential barrier alone. However, unlike Toho/CEX, we note that the ChElPG charge profiles in Toho/AMP acylation demonstrate a similar pattern for the R1 and R2 pathways (Fig. 3b, 3c), suggesting that the R1 acylation mechanism is at least competitive to the R2 alternatives. The viability of both R1 and R2 pathways in Toho-1 mediated β-lactam acylation was also supported by

pioneering computational[6,8] and experimental[15] studies. In our assessment, the acylation mechanism developed for ASβLs/benzylpenicillin, where both acylation pathways are accessible, is naturally transferable to Toho/AMP catalysis. However, the acylation pathway utilizing Glu166 as the general base was shown to be kinetically prohibitive for Toho/CEX as a result of the extended delocalization on N5, which is introduced by the C3=C4 double bond. The viable acylation pathway for CEX is thus the Lys73/Glu166 dual base mechanism.

Our calculations with CEX acylation also shed light onto the hydrolysis of other cephalosporins. As noted above, CEX mechanistically stands out in the cephalosporin family as its β-lactam nitrogen has to be protonated upon the formation of the acyl-enzyme product. However, common cephalosporins such as cephalothin and cefotaxime show higher catalytic efficiency (k_{cat}/K_M)[9,16,17], which suggests a much lower acylation barrier than that of CEX. Such observations suggest that the cephem nitrogen may not be protonated during the entire acylation processes of other cephalosporins. Through their crystallographic study, Olmos *et al*.[18] recently observed that the departure of the C3' leaving group is clearly simultaneous to the serine attack during the ASβLs/cefotaxime acylation, supporting the above hypothesis. In this regard, the protonation of the cephem nitrogen, which was also previously validated as the rate limiting step[11], could be avoided, and leading to the higher acylation rates observed in other early generations of cephalosporins.

Currently, efficient mechanism-based development of new antibiotics is obstructed by the lack of sufficient knowledge on the energetic landscapes of various β-lactam hydrolysis. In the present study, we report that one enzyme can adopt different acylation pathways responding to different substrate structures. Using AMP and CEX as the model substrates and Toho-1 as the enzyme, our QM/MM CoS pathway calculations demonstrated that the acylation mechanism of Toho-1 can be substrate-dependent. The acylation pathways with Glu166 acting as the only general base are shown to be viable for AMP but

prohibitive for CEX. We attribute the low acylation activity in CEX to the lowered proton affinity of the β-lactam nitrogen induced by the extended π-conjugation from the dihydrothiazine ring. In this regard, the reactivity of the scissile C–N bond could be engineered by introducing additional π-conjugations to the β-lactam. Accordingly, we note that similar structural features can also be seen on other robust β-lactam variants (such as carbapenems and aza-β-lactams[19,41]). In conclusion, we report the distinct mechanistic basis of the seemingly identical acylation barrier for Toho-1 mediated AMP and CEX hydrolysis. On the basis of the comparative mechanistic analysis to Toho/AMP and Toho/CEX acylation profiles, it is expected that the current study enlightens the flexibility of the ASβLs mediated β-lactam acylation and could facilitate future optimization and development of β-lactam based antibiotic drugs.

References

(1) Fisher, J. F.; Meroueh, S. O.; Mobashery, S. Bacterial Resistance to β-Lactam Antibiotics: Compelling Opportunism, Compelling Opportunity. *Chem. Rev.* **2005**, *105* (2), 395–424. https://doi.org/10.1021/cr030102i.

(2) Drawz, S. M.; Bonomo, R. A. Three Decades of β-Lactamase Inhibitors. *Clin. Microbiol. Rev.* **2010**, *23* (1), 160–201. https://doi.org/10.1128/CMR.00037-09.

(3) Llarrull, L. I.; Testero, S. A.; Fisher, J. F.; Mobashery, S. The Future of the β-Lactams. *Curr. Opin. Microbiol.* **2010**, *13* (5), 551–557. https://doi.org/10.1016/j.mib.2010.09.008.

(4) Cantón, R.; González-Alba, J. M.; Galán, J. C. CTX-M Enzymes: Origin and Diffusion. *Front. Microbiol.* **2012**, *3*, 110–110. https://doi.org/10.3389/fmicb.2012.00110.

(5) Palzkill, T. Structural and Mechanistic Basis for Extended-Spectrum Drug-Resistance Mutations in Altering the Specificity of TEM, CTX-M, and KPC β-Lactamases. *Front. Mol. Biosci.* **2018**, *5*, 16. https://doi.org/10.3389/fmolb.2018.00016.

(6) Hermann, J. C.; Hensen, C.; Ridder, L.; Mulholland, A. J.; Höltje, H.-D. Mechanisms of Antibiotic Resistance: QM/MM Modeling of the Acylation Reaction of a Class A β-Lactamase with Benzylpenicillin. *J. Am. Chem. Soc.* **2005**, *127* (12), 4454–4465. https://doi.org/10.1021/ja044210d.

(7) Hermann, J. C.; Ridder, L.; Höltje, H.-D.; Mulholland, A. J. Molecular Mechanisms of Antibiotic Resistance: QM/MM Modelling of Deacylation in a Class A β-Lactamase. *Org Biomol Chem* **2006**, *4* (2), 206–210. https://doi.org/10.1039/B512969A.

(8) Meroueh, S. O.; Fisher, J. F.; Schlegel, H. B.; Mobashery, S. Ab Initio QM/MM Study of Class A β-Lactamase Acylation: Dual Participation of Glu166 and Lys73 in a Concerted Base Promotion of Ser70. *J. Am. Chem. Soc.* **2005**, *127* (44), 15397–15407. https://doi.org/10.1021/ja051592u.

(9) Nitanai, Y.; Shimamura, T.; Uchiyama, T.; Ishii, Y.; Takehira, M.; Yutani, K.; Matsuzawa, H.; Miyano, M. The Catalytic Efficiency (Kcat/Km) of the Class A β-Lactamase Toho-1 Correlates with the Thermal Stability of Its Catalytic Intermediate Analog. *Biochim. Biophys. Acta BBA - Proteins Proteomics* **2010**, *1804* (4), 684–691. https://doi.org/10.1016/j.bbapap.2009.10.023.

(10) Langan, P. S.; Vandavasi, V. G.; Weiss, K. L.; Cooper, J. B.; Ginell, S. L.; Coates, L. The Structure of Toho1 β-Lactamase in Complex with Penicillin Reveals the Role of Tyr105 in Substrate Recognition. *FEBS Open Bio* **2016**, *6* (12), 1170–1177. https://doi.org/10.1002/2211-5463.12132.

(11) Song, Z.; Zhou, H.; Tian, H.; Wang, X.; Tao, P. Unraveling the Energetic Significance of Chemical Events in Enzyme Catalysis via Machine-Learning Based Regression Approach. *Commun. Chem.* **2020**, *3* (1), 134. https://doi.org/10.1038/s42004-020-00379-w.

(12) Vandavasi, V. G.; Weiss, K. L.; Cooper, J. B.; Erskine, P. T.; Tomanicek, S. J.; Ostermann, A.; Schrader, T. E.; Ginell, S. L.; Coates, L. Exploring the Mechanism of β-Lactam Ring Protonation in the Class A β-Lactamase Acylation Mechanism Using Neutron and X-Ray Crystallography. *J. Med. Chem.* **2016**, *59* (1), 474–479. https://doi.org/10.1021/acs.jmedchem.5b01215.

(13) Shimizu-Ibuka, A.; Oishi, M.; Yamada, S.; Ishii, Y.; Mura, K.; Sakai, H.; Matsuzawa, Hiroshi. Roles of Residues Cys69, Asn104, Phe160, Gly232, Ser237, and Asp240 in Extended-Spectrum β-Lactamase Toho-1. *Antimicrob. Agents Chemother.* **2011**, *55*, 284–290. https://doi.org/10.1128/AAC.00098-10.

(14) Langan, P. S.; Vandavasi, V. G.; Cooper, S. J.; Weiss, K. L.; Ginell, S. L.; Parks, J. M.; Coates, L. Substrate Binding Induces Conformational Changes in a Class A β-Lactamase That Prime It for Catalysis. *ACS Catal.* **2018**, *8*, 2428–2437. https://doi.org/10.1021/acscatal.7b04114.

(15) Tomanicek, S. J.; Wang, K. K.; Weiss, K. L.; Blakeley, M. P.; Cooper, J.; Chen, Y.; Coates, Leighton. The Active Site Protonation States of Perdeuterated Toho-1 β-Lactamase Determined by Neutron Diffraction Support a Role for Glu166 as the General Base in Acylation. *FEBS Lett.* **2011**, *585*, 364–368. https://doi.org/10.1016/j.febslet.2010.12.017.

(16) Shimamura, T.; Ibuka, A.; Fushinobu, S.; Wakagi, T.; Ishiguro, M.; Ishii, Y.; Matsuzawa, H. Acyl-Intermediate Structures of the Extended-Spectrum Class A β-Lactamase, Toho-1, in Complex with Cefotaxime, Cephalothin, and Benzylpenicillin. *J. Biol. Chem.* **2002**, *277* (48), 46601–46608.

(17) Adamski, C. J.; Cardenas, A. M.; Brown, N. G.; Horton, L. B.; Sankaran, B.; Prasad, B. V. V.; Gilbert, H. F.; Palzkill, T. Molecular Basis for the Catalytic Specificity of the CTX-M Extended-Spectrum β-Lactamases. *Biochemistry* **2015**, *54* (2), 447–457. https://doi.org/10.1021/bi501195g.

(18) Olmos, J. L.; Pandey, S.; Martin-Garcia, J. M.; Calvey, G.; Katz, A.; Knoska, J.; Kupitz, C.; Hunter, M. S.; Liang, M.; Oberthuer, D.; Yefanov, O.; Wiedorn, M.; Heyman, M.; Holl, M.; Pande, K.; Barty, A.; Miller, M. D.; Stern, S.; Roy-Chowdhury, S.; Coe, J.; Nagaratnam, N.; Zook, J.; Verburgt, J.; Norwood, T.; Poudyal, I.; Xu, D.; Koglin, J.; Seaberg, M. H.; Zhao, Y.; Bajt, S.; Grant, T.; Mariani, V.; Nelson, G.; Subramanian, G.; Bae, E.; Fromme, R.; Fung, R.; Schwander, P.; Frank, M.; White, T. A.; Weierstall, U.; Zatsepin, N.; Spence, J.; Fromme, P.; Chapman, H. N.;

Pollack, L.; Tremblay, L.; Ourmazd, A.; Phillips, G. N.; Schmidt, M. Enzyme Intermediates Captured "on the Fly" by Mix-and-Inject Serial Crystallography. *BMC Biol.* **2018**, *16* (1), 59. https://doi.org/10.1186/s12915-018-0524-5.

(19) Das, C. K.; Nair, N. N. Elucidating the Molecular Basis of Avibactam-Mediated Inhibition of Class A B-Lactamases. *Chem. – Eur. J.* **2020**, *26* (43), 9639–9651. https://doi.org/10.1002/chem.202001261.

(20) Hoemann, M. Z. Penicillin and Cephalosporin Antibiotics. In *Bioactive Heterocyclic Compound Classes*; Dinges, J., Lamberth, C., Eds.; Wiley-VCH Verlag GmbH & Co. KGaA: Weinheim, Germany, 2013; pp 237–253. https://doi.org/10.1002/9783527664450.ch15.

(21) Brokaw, J. B.; Haas, K. R.; Chu, J.-W. Reaction Path Optimization with Holonomic Constraints and Kinetic Energy Potentials. *J. Chem. Theory Comput.* **2009**, *5* (8), 2050–2061. https://doi.org/10.1021/ct9001398.

(22) Woodcock, H. L.; Hodošček, M.; Sherwood, P.; Lee, Y. S.; Schaefer III, H. F.; Brooks, B. R. Exploring the Quantum Mechanical/Molecular Mechanical Replica Path Method: A Pathway Optimization of the Chorismate to Prephenate Claisen Rearrangement Catalyzed by Chorismate Mutase. *Theor. Chem. Acc.* **2003**, *109* (3), 140–148. https://doi.org/10.1007/s00214-002-0421-3.

(23) E, W.; Ren, W.; Vanden-Eijnden, E. String Method for the Study of Rare Events. *Phys. Rev. B* **2002**, *66* (5), 052301. https://doi.org/10.1103/PhysRevB.66.052301.

(24) Tao, P.; Hodošček, M.; Larkin, J. D.; Shao, Y.; Brooks, B. R. Comparison of Three Chain-of-States Methods: Nudged Elastic Band and Replica Path with Restraints or Constraints. *J. Chem. Theory Comput.* **2012**, *8* (12), 5035–5051. https://doi.org/10.1021/ct3006248.

(25) Vanommeslaeghe, K.; Hatcher, E.; Acharya, C.; Kundu, S.; Zhong, S.; Shim, J.; Darian, E.; Guvench, O.; Lopes, P.; Vorobyov, I.; Mackerell Jr., A. D. CHARMM General Force Field: A Force Field for Drug-like Molecules Compatible with the CHARMM All-Atom Additive Biological Force Fields. *J. Comput. Chem.* **2010**, *31* (4), 671–690. https://doi.org/10.1002/jcc.21367.

(26) Vanommeslaeghe, K.; MacKerell, A. D. Automation of the CHARMM General Force Field (CGenFF) I: Bond Perception and Atom Typing. *J. Chem. Inf. Model.* **2012**, *52* (12), 3144–3154. https://doi.org/10.1021/ci300363c.

(27) Vanommeslaeghe, K.; Raman, E. P.; MacKerell, A. D. Automation of the CHARMM General Force Field (CGenFF) II: Assignment of Bonded Parameters and Partial Atomic Charges. *J. Chem. Inf. Model.* **2012**, *52* (12), 3155–3168. https://doi.org/10.1021/ci3003649.

(28) Gaus, M.; Cui, Q.; Elstner, M. DFTB3: Extension of the Self-Consistent-Charge Density-Functional Tight-Binding Method (SCC-DFTB). *J. Chem. Theory Comput.* **2011**, *7* (4), 931–948. https://doi.org/10.1021/ct100684s.

(29) Gaus, M.; Goez, A.; Elstner, M. Parametrization and Benchmark of DFTB3 for Organic Molecules. *J. Chem. Theory Comput.* **2013**, *9* (1), 338–354. https://doi.org/10.1021/ct300849w.

(30) Best, R. B.; Zhu, X.; Shim, J.; Lopes, P. E. M.; Mittal, J.; Feig, M.; MacKerell, A. D. Optimization of the Additive CHARMM All-Atom Protein Force Field Targeting Improved Sampling of the Backbone ϕ, ψ and Side-Chain X1 and X2 Dihedral Angles. *J. Chem. Theory Comput.* **2012**, *8* (9), 3257–3273. https://doi.org/10.1021/ct300400x.

(31) Becke, A. D. A New Mixing of Hartree–Fock and Local Density-functional Theories. *J. Chem. Phys.* **1993**, *98* (2), 1372–1377. https://doi.org/10.1063/1.464304.

(32) Ditchfield, R.; Hehre, W. J.; Pople, J. A. Self-Consistent Molecular-Orbital Methods. IX. An Extended Gaussian-Type Basis for Molecular-Orbital Studies of Organic Molecules. *J. Chem. Phys.* **1971**, *54* (2), 724–728. https://doi.org/10.1063/1.1674902.

(33) Brooks, B. R.; Brooks III, C. L.; Mackerell Jr., A. D.; Nilsson, L.; Petrella, R. J.; Roux, B.; Won, Y.; Archontis, G.; Bartels, C.; Boresch, S.; Caflisch, A.; Caves, L.; Cui, Q.; Dinner, A. R.; Feig, M.; Fischer, S.; Gao, J.; Hodoscek, M.; Im, W.; Kuczera, K.; Lazaridis, T.; Ma, J.; Ovchinnikov, V.; Paci, E.; Pastor, R. W.; Post, C. B.; Pu, J. Z.; Schaefer, M.; Tidor, B.; Venable, R. M.; Woodcock, H. L.; Wu, X.; Yang, W.; York, D. M.; Karplus, M. CHARMM: The Biomolecular Simulation Program. *J. Comput. Chem.* **2009**, *30* (10), 1545–1614. https://doi.org/10.1002/jcc.21287.

(34) Woodcock, H. L.; Hodošček, M.; Gilbert, A. T. B.; Gill, P. M. W.; Schaefer III, H. F.; Brooks, B. R. Interfacing Q-Chem and CHARMM to Perform QM/MM Reaction Path Calculations. *J. Comput. Chem.* **2007**, *28* (9), 1485–1502. https://doi.org/10.1002/jcc.20587.

(35) Epifanovsky, E.; Gilbert, A. T. B.; Feng, X.; Lee, J.; Mao, Y.; Mardirossian, N.; Pokhilko, P.; White, A. F.; Coons, M. P.; Dempwolff, A. L.; Gan, Z.; Hait, D.; Horn, P. R.; Jacobson, L. D.; Kaliman, I.; Kussmann, J.; Lange, A. W.; Lao, K. U.; Levine, D. S.; Liu, J.; McKenzie, S. C.; Morrison, A. F.; Nanda, K. D.; Plasser, F.; Rehn, D. R.; Vidal, M. L.; You, Z.-Q.; Zhu, Y.; Alam,

B.; Albrecht, B. J.; Aldossary, A.; Andersen, J. H.; Athavale, V.; Barton, D.; Begam, K.; Behn, A.; Bernard, Y. A.; Berquist, E. J.; Burton, H. G. A.; Carreras, A.; Carter-Fenk, K.; Chien, A. D.; Closser, K. D.; Cofer-Shabica, V.; Dasgupta, S.; de Wergifosse; Deng, J.; Diedenhofen, M.; Do, H.; Ehlert, S.; Fang, P.-T.; Feng, Q.; Friedhoff, T.; Gayvert, J.; Ge, Q.; Gidofalvi, G.; Goldey, M.; González-Espinoza, C. E.; Gulania, S.; Gunina, A. O.; Hanson, M. W. D.; Harbach, P. H. P.; Hauser, A.; Herbst, M. F.; Vera, M. H.; Holden, Z. C.; Houck, S.; Huang, X.; Hui, K.; Huynh, B. C.; Ivanov, M.; Jász, Á.; Ji, H.; Jiang, H.; Kaduk, B.; Kähler, S.; Khistyaev, K.; Kim, J.; Kis, G.; Klunzinger, P.; Koczor-Benda, Z.; Koh, J. H.; Kosenkov, D.; Koulias, L.; Kowalczyk, T.; Krauter, C. M.; Kue, K.; Kunitsa, A.; Kus, T.; Ladjánszki, I.; Landau, A.; Lawler, K. V.; Lefrancois, D.; Lehtola, S.; Li, R. R.; Li, Y.-P.; Liang, J.; Liebenthal, M.; Lin, H.-H.; Lin, Y.-S.; Liu, F.; Liu, K.-Y.; Loipersberger, M.; Manjanath, A.; Manohar, P.; Mansoor, E.; Manzer, S. F.; Mao, S.-P.; Marenich, V.; Markovich, T.; Mason, S.; Maurer, S. A.; McLaughlin, P. F.; Mewes, J.-M.; Mewes, S. A.; Morgante, P.; Mullinax, J. W.; Oosterbaan, J.; Paran, G.; Paul, A. C.; Paul, S. K.; Pavošević, F.; Pei, Z.; Prager, S.; Proynov, E. I.; Rák, Á.; Ramos-Cordoba, E.; Rana, B.; Rask, A. E.; Richard, R. M.; Rob, F.; Rossomme, E.; Scheele, T.; Scheurer, M.; Sergueev, N.; Sharada, S. M.; Skomorowski, W.; Small, D. W.; Stein, J.; Su, Y.-C.; Sundstrom, E. J.; Tao, Z.; Thirman, J.; Tornai, G. J.; Tubman, N. M.; Veccham, S. P.; Vydrov, O.; Wenzel, J.; Witte, J.; Yamada, A.; Yao, K.; Yeganeh, S.; Yost, S. R.; Zech, A.; Zhang, I. Y.; Zhang, Y.; Zuev, D.; Aspuru-Guzik, A.; Bell, A. T.; Besley, N. A.; Bravaya, K. B.; Brooks, B. R.; Casanova, D.; Chai, J.-D.; Coriani, S.; Cramer, C. J.; DePrince, A. E.; DiStasio, R. A.; Dreuw, A.; Dunietz, B. D.; Goddard, W. A.; Hammes-Schiffer, S.; Head-Gordon, T.; Hehre, W. J.; Hsu, P.; Jagau, T.-C.; Jung, Y.; Klamt, A.; Kong, J.; Lambrecht, D. S.; Mayhall, N. J.; McCurdy, C. W.; Neaton, J. B.; Ochsenfeld, C.; Peverati, R.; Rassolov, V. A.; Shao, Y.; Slipchenko, L. V.; Stauch, T.; Steele, R. P.; Subotnik, J. E.; Thom, A. J. W.; Tkatchenko, A.; Truhlar, D. G.; Voorhis, V.; Wesolowski, T. A.; Whaley, K. B.; Woodcock, H. L.; Zimmerman, P. M.; Faraji, S.; Gill, P. M. W.; Head-Gordon, M.; Herbert, J. M.; Krylov, A. I. Software for the Frontiers of Quantum Chemistry: An Overview of Developments in the Q-Chem 5 Package. *J. Chem. Phys.* **2021**, 61.

(36) Hehre, W. J.; Ditchfield, R.; Pople, J. A. Self-Consistent Molecular Orbital Methods. XII. Further Extensions of Gaussian—Type Basis Sets for Use in Molecular Orbital Studies of Organic Molecules. *J. Chem. Phys.* **1972**, *56* (5), 2257–2261. https://doi.org/10.1063/1.1677527.

(37) Lonsdale, R.; Harvey, J. N.; Mulholland, A. J. Inclusion of Dispersion Effects Significantly Improves Accuracy of Calculated Reaction Barriers for Cytochrome P450 Catalyzed Reactions. *J. Phys. Chem. Lett.* **2010**, *1* (21), 3232–3237. https://doi.org/10.1021/jz101279n.

(38) Lonsdale, R.; Harvey, J. N.; Mulholland, A. J. Effects of Dispersion in Density Functional Based Quantum Mechanical/Molecular Mechanical Calculations on Cytochrome P450 Catalyzed Reactions. *J. Chem. Theory Comput.* **2012**, *8* (11), 4637–4645. https://doi.org/10.1021/ct300329h.

(39) Grimme, S. Semiempirical GGA-Type Density Functional Constructed with a Long-Range Dispersion Correction. *J. Comput. Chem.* **2006**, *27* (15), 1787–1799. https://doi.org/10.1002/jcc.20495.

(40) Breneman, C. M.; Wiberg, K. B. Determining Atom-Centered Monopoles from Molecular Electrostatic Potentials. The Need for High Sampling Density in Formamide Conformational Analysis. *J. Comput. Chem.* **1990**, *11* (3), 361–373. https://doi.org/10.1002/jcc.540110311.

(41) Nangia, A.; Chandrakala, P. S. Synthesis of 1,3-Diazetidin-2-Ones (Aza-β-Lactams) as Rationally Designed Transpeptidase and β-Lactamase Inhibitors. *Tetrahedron Lett.* **1995**, *36* (42), 7771–7774. https://doi.org/10.1016/0040-4039(95)01473-U.

Acknowledgement

This material is based upon work supported by the National Science Foundation under a CAREER Grant No. 1753167. T.P. is supported by NIH grant AI32956. Computational time was provided by the Southern Methodist University's Centre for Research Computing.

Conflict of Interest

The authors declare no competing financial interest.